Influence of Alkyl Peptidoamines on the Structure of Functionalized Mesoporous Silica

J. L. Blin,*,† C. Gérardin,‡ L. Rodehüser,‡ C. Selve,‡ and M. J. Stébé†

Equipe Physico-chimie des Colloïdes and Equipe Matériaux Tensioactifs, Polymères et Colloïdaux, UMR 7565 Université Nancy 1/CNRS, Faculté des Sciences, BP 239, F-54506 Vandoeuvre-les-Nancy Cedex, France

Received April 1, 2004. Revised Manuscript Received September 2, 2004

The functionalization of mesoporous silica materials with alkyl peptidoamines by the co-condensation method was investigated. Alkylpeptidoamines were introduced via (aminopropyl)triethoxysilane (APTES). Samples were prepared by using a nonionic fluorinated surfactant $CF_3(CF_2)_7C_2H_4(OC_2H_4)_9OH$. Results obtained by SAXS and nitrogen adsorption−desorption analysis clearly showed that the channel arrangement of the recovered materials depends not only on the organosilane/(organosilane+tetramethyl orthosilicate) molar fraction but also on the nature of the functional groups. Indeed, materials functionalized with BOC-Phe-APTES or with small amounts of BOC-Glu(αOBn)-βAla-APTES exhibit a hexagonal channel array. Higher BOC-Glu(αOBn)-βAla-APTES loading leads to a wormhole-like mesostructure. Whatever the organosilane/(organosilane+tetramethyl orthosilicate) molar fraction, only disordered structures are recovered when functionalization is performed with Z-Asp(αOBn)-APTES. Moreover, the pore wall thickness is strongly affected by the structure of the organic groups. The efficiency of the functionalization was evidenced by FTIR and solid state ^{29}Si and ^{13}C MAS NMR spectroscopies. Results obtained from solid state ^{29}Si NMR also show that polymerization rates of organosilane and tretramethyl orthosilicate must be very close to each other.

1. Introduction

Organic−inorganic hybrid materials are of particular interest in the preparation of catalysts,[1−3] drug delivery systems,[4] and sensors.[5] Their expansion is due to the development of soft chemical processes, such as sol−gel chemistry. Materials can be prepared by postsynthesis grafting of an organic compound, such as an organoalkoxysilane, on a substrate. In this case weak interactions such as hydrogen bonding, van der Waals, or electrostatic forces, occur between the organic and inorganic phases. Another method to synthesize those materials consists of the cohydrolysis and polycondensation of an alkoxysilane, for instance tetramethyl orthosilicate (TMOS), and an organoalkoxysilane. This second pathway involves a covalent link between both moieties. Recently our group reported the synthesis of functionalized silica obtained by copolymerization of silyloxyalkylamidocarnosine and tetraalkoxysilanes,[6] where we have shown that these organo-mineral solids are good ligands for metal cations (Cu^{2+} or Zn^{2+}). However, control over the pore size distribution of the sol−gel is difficult, which from the complexation point of view constitutes the main disadvantage of the process as it prevents high selectivity. Owing to their properties such as high specific surface area and uniform pore size distribution, mesoporous materials can overcome this drawback.[7,8]

The synthesis of pure silica mesoporous molecular sieves consists of the condensation and polymerization of an inorganic source of silica around the micelles of surfactants. The synthesis can be achieved through either an electrostatic pathway,[7−12] based on a supramolecular assembly of charged surfactants with charged inorganic precursors, or a neutral pathway,[13−15] in which hydrogen bonding is responsible for the

* To whom correspondence should be addressed. Phone: +33-3-83-68-43-70. Fax: +33-3-83-68-43-22. E-mail: Jean-Luc.Blin@lesoc.uhp-nancy.fr.
† Equipe Physico-chimie des Colloïdes.
‡ Equipe Matériaux Tensioactifs, Polymères et Colloïdaux.

(1) Clerici, M. G. *Appl. Catal.* **1991**, *68*, 249.
(2) Clerici, M. G.; Ingallina, P. *J. Catal.* **1993**, *140*, 71.
(3) Nakamura, S.; Yasui, T. *J. Catal.* **1970**, *17*, 336.
(4) Vallet-Regi, M.; Ramila, A.; Del Real, R. P.; Pérez-Pariente, J. *Chem. Mater.* **2001**, *13*, 308.
(5) Walcarius, A.; Lüthi, N.; Blin, J. L.; Su, B. L.; Lamberts, L. *Electrochim. Acta* **1999**, *44*, 4601.
(6) Hamdoune, F.; El Moujahid, C.; Stébé, M. J.; Gérardin, C.; Tekely, P.; Selve, C.; Rodehüser, L. *Prog. Colloid Polym. Sci.* **2001**, *118*, 107.
(7) Kresge, C. T.; Leonowicz, M. E.; Roth, W. J.; Vartuli, J. C.; Beck, J. S. *Nature* **1992**, *359*, 710.
(8) Beck, J. S.; Vartuli, J. C.; Roth, W. J.; Leonowicz, M. E.; Kresge, C. T.; Schmitt, K. D.; Chu, C. T. W.; Olson, D. H.; Sheppard, E. W.; McCulle, S. B.; Higgins, J. B.; Schlender, J. L. *J. Am. Chem. Soc.* **1992**, *114*, 10834.
(9) Huo, Q.; Margolese, D. I.; Ciesla, U.; Feng, P.; Gier, T. E.; Sieger, P.; Leon, R.; Petroff, P. M.; Schüth, F.; Stucky G. D. *Nature* **1994**, *368*, 317.
(10) Chen, C. Y.; Li, H. Y.; Davis, M. E. *Microporous Mater*. **1993**, *2*, 17.
(11) Chen, C. Y.; Li, H. Y.; Burkett, S. L.; Davis, M. E. *Microporous Mater.* **1993**, *2*, 27.
(12) Huo, Q.; Margolese, D. I.; Ciesla, U.; Demuth, D. G.; Feng, P.; Gier, T. E.; Sieger, P.; Firouzi, A.; Chmelka, B. F.; Schüth, F.; Stucky, G. D. *Chem. Mater.* **1994**, *6*, 1176.
(13) Sayari, A. *Stud. Surf. Sci. Catal.* **1996**, *102*, 1.
(14) Tanev, P. T.; Pinnavaia, T. J. *Science* **1995**, *267*, 865.
(15) Tanev, P. T.; Pinnavaia, T. J. *Chem. Mater.* **1996**, *8*, 2068.

10.1021/cm049452r CCC: $27.50
Published on Web 10/28/2004

Table 1. Structure of Silylated Alkyl Peptidoamine Monomers

Compound no.	Abbreviation	Structure
1	Z-Asp(αOBn)-APTES	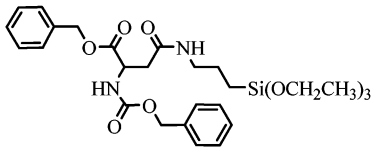
2	BOC-Glu(αOBn)-βAla-APTES	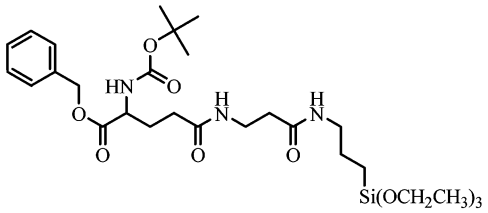
3	BOC-Phe-APTES	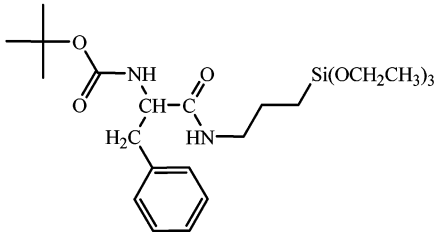

cohesiveness between the surfactant and the inorganic precursor. Different kinds of materials called MCM (Mobil crystalline materials),[7,8] SBA (Santa Barbara),[16] or MSU (Michigan State University)[17] have been obtained via an electrostatic route for MCM and a neutral pathway for the others. The surface of mesoporous silica is considered to be covered with silanol groups and can be modified. Functionalization of these ordered mesoporous molecular sieves via the postsynthesis method was investigated.[18−21] However, neither the concentration nor the distribution of the organic group can be controlled by grafting; this is why much attention has been paid to the co-condensation method.[22−27]

For example, Zhao et al.[28] reported the functionalization of SBA-15 with an amine moiety which is an important prosthetic group for many applications such as enzyme immobilization on porous solid support. The authors conclude that the co-condensation method allows a better control of the pore size and the density of functional groups. However, the channel arrangement strongly depends on the molar ratio between the two silica sources. Using different surfactants, Corriu et al.[29] described a general method to prepare mesoporous materials containing cyclam. By means of $CuCl_2$ and $CoCl_2$ complexation, the authors proved that all the cyclam moieties located inside the channel pores are accessible. More recently, the preparation of dipeptide-functionalized mesoporous silica spheres has been reported.[30] The synthesis was achieved by co-condensation of carnosine-containing triethoxysilane and tetraethoxysilane, in basic hydro alcoholic medium, using cetyltrimethylammonium bromide as surfactant. Recovered materials exhibit a wormhole-like structure.

To develop silica matrixes for biomolecule encapsulation or metal cation complexation, in the present work we use peptidoamides to functionalize mesoporous materials by co-condensation of organosilanes and tetramethoxysilane (TMOS). As mentioned above, the amine group is very interesting for such applications. The synthesis is performed under neutral pH conditions, using a nonionic fluorinated surfactant, $CF_3(CF_2)_7C_2H_4(OC_2H_4)_9OH$. In a previous publication,[31] we have shown that the use of this surfactant leads to mesoporous materials of well-defined structure, high specific surface area, and pore diameter up to 5.0 nm. Moreover, with nonionic surfactant, solvent extraction by ethanol instead of calcination can be chosen to free the pores.

We have investigated the influence of the molar ratio of organosilane to TMOS on the structural and textural properties of the mesoporous silica. Three different monomers, represented in Table 1, have been used for the preparation of the mesoporous material.

2. Materials and Methods

2.1. Organic Precursor Preparation. *2.1.1. Chemicals and Reagents.* Solvents were reagent grade and used without

(16) Huo, Q.; Margolese, D. I.; Stucky, G. D. *Chem. Mater.* **1996**, *8*, 1147.
(17) Bagshaw, S. A.; Prouzet, E.; Pinnavaia, T. J. *Science* **1995**, *269*, 1242.
(18) Mercier, L.; Pinnavaia, T. J. *Adv. Mater.* **1997**, *9*, 500.
(19) Brunel, D.; Cauvel, A.; Di Renzo, F.; Fajula, F.; Fubini, B.; Onida, B.; Garrone, E. *New J. Chem.* **2000**, *24*, 807.
(20) Price, P. M.; Clark, J. H.; Macquarrie, D. J. *J. Chem. Soc. Dalton Trans.* **2000**, 101.
(21) Liu, A. M.; Hidajat, K.; Kawi, S.; Zhao, D. Y. *Chem. Commun.* **2000**, 1145.
(22) Burleigh, M. C.; Markowitz, M. A.; Spector, M. S.; Gaber, B. P. *J. Phys. Chem. B* **2001**, *105*, 9935.
(23) Richer, R.; Mercier, L. *Chem. Commun.* **1998**, 1775.
(24) Marcquarrie, D. J. *Green Chem.* **1999**, 195.
(25) Huh, S.; Wiench, J. W.; Yoo, J. C.; Pruski, M.; Lin, V. S. Y. *Chem. Mater.* **2003**, *15*, 4247.
(26) Marcquarrie, D. J.; Jackson, D. B.; Mdoe, J. E. G.; Clark, J. H. *New J. Chem.* **1999**, *23*, 539.
(27) Kosuge, K.; Murakami, T.; Kikukawa, N.; Takemori, M. *Chem. Mater.* **2003**, *15*, 3134.
(28) Chong, A. S. M.; Zhao, X. S. *J. Phys. Chem. B* **2003**, *107*, 12650.
(29) Corriu, R. J. P.; Mehdi, A.; Reyé, C.; Thieuleux, C. *Chem. Mater.* **2004**, *16*, 159.
(30) Walcarius, A.; Sayen, S.; Gérardin, C.; Hamdoune, F.; Rodehüser, L. *Colloids Surf., A* **2004**, *234*, 145.
(31) Blin, J. L.; Lesieur, P.; Stébé, M. J. *Langmuir* **2004**, *20*, 491.

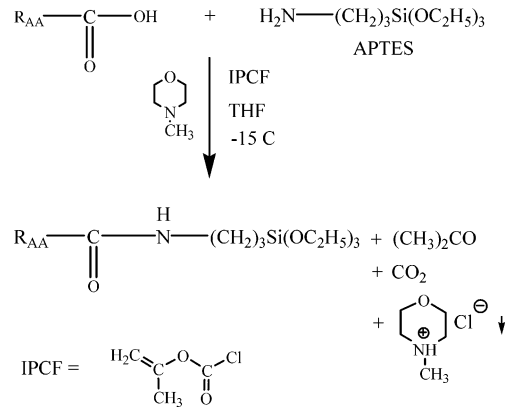

Figure 1. Scheme of the coupling between the amino group of 3-aminopropyl-triethoxysilane (APTES) and the carboxyl group of the selected amino acid.

further purification, except for tetrahydrofuran (THF) and diethyl ether which were dehydrated by distillation from sodium wire.

The progress of reactions and the purity of products were evaluated on thin layer silica gel chromatographic (TLC) plates (Merck, Kieselgel 60 F254) with ethyl-acetate/hexane or chloroform/methanol as eluents.

2.1.2. Analyses. The proton (^{1}H) NMR spectra were recorded on a Bruker AM 400 or AC 200 spectrometer, and the ^{29}Si and ^{13}C spectra of solid samples were recorded on a Bruker 300 apparatus. The chemical shifts (δ) are reported in parts per million (δ in ppm) downfield from tetramethylsilane (TMS). The IR spectra were recorded on a Perkin-Elmer (Spectrum one) FTIR spectrometer.

2.1.3. Synthesis of Silylated Monomers. Mesoporous silica samples were obtained by copolymerization of a functionalized silylated monomer and TMOS under sol−gel conditions in the presence of a nonionic surfactant.

The functionalized silylated monomer was prepared by amide coupling between the amino group of 3-aminopropyl-triethoxysilane (APTES) and the carboxyl group of a selected amino acid as shown in Figure 1. For this reaction, the other functional groups of the amino acid had to be protected to avoid undesired byproducts. The protecting groups chosen were *tert*-butyloxycarbonyl (BOC) or benzyloxycarbonyl (Z) for $-NH_2$, and methyl (OMe) or benzyl-ester (OBn) groups for the carboxyl function.

To avoid the solvolysis of the precursor during synthesis, which would lead to uncontrolled polymerization, it is necessary to preclude the introduction of water or alcohols, even in trace amounts. Therefore isopropenyl-chloroformate (IPCF) was chosen as coupling reagent, yielding easily removable byproducts such as acetone and carbon dioxide during the reaction. An excess of the agent itself can easily be evaporated under reduced pressure. Hydrochloric acid generated during the synthesis is trapped with *N*-methyl-morpholine; the hydrochloride formed is removed by treatment with diethyl ether.

The introduction of different amino acid substituents R_{AA} leads to the silylated monomers shown in Table 1.

The preparation of the precursors is described in detail below.

*(a) Z-Asp(αOBn)-APTES (**1**).* Z-Asp(αOBn)OH (2 mMol

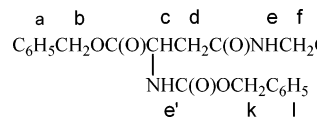

(0.715 g)) was dissolved in 30 mL of THF. At −15 °C 1 equiv (2 mMol, 0.061 g) of *N*-methylmorpholine was added under stirring in a dry argon atmosphere, followed by 1 equiv (0.0724 g) of isopropenyl-chloroformate and 1 equiv (0.1325 g) of APTES. After 4 h the precipitate of *N*-methylmorpholinium chloride was filtered off and the solvent was evaporated under vacuum. The product, a slightly yellow viscous oil, was kept under dry argon. Yield 0.98 g (87%).

IR: $\nu_{[NH]}$ 3200−3400 cm^{-1}, $\nu_{[CO]}$ 1645 cm^{-1}, $\nu_{[CO]}$ 1700 cm^{-1}, $\nu_{[CO]}$ 1710 cm^{-1}. ^{1}H NMR: 3.2 (2H, m, f); 1.65 (2H, m, g); 0.65 (2H, m, h); 4.4 (6H, q, J = 6.8 Hz, i); 1.2 (9H, t, J = 6.8 Hz, j).

*(b) BOC-Glu(αOBn)-βAla-APTES (**2**).* This compound was

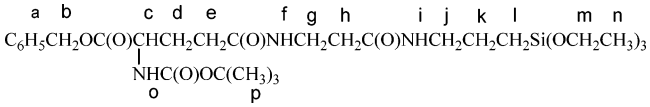

synthesized in three steps. First, a peptide coupling between β-alanine-methyl ester hydrochloride (1.39 g, 10 mMol) and BOC glutamic acid (αOBn) (3.37 g, 10 mMol) in 70 mL of acetonitrile with BOP (4.42 g, 10 mMol) as coupling reagent, in the presence of 3 equiv (3.03 g) of triethylamine, led to the dipeptide BOC-Glu(αOBn)-βAla(OMe) after 12 h of continuous stirring. In the second step the methyl ester group was removed by treatment with 5 equiv of 5N NaOH in a methanol−water mixture (90:10 w/w). After acidification to pH 2 and evaporation of methanol, the aqueous phase was extracted twice with CH_2Cl_2; the latter was distilled off after dehydration over $MgSO_4$ to yield 3.33 g (81%) of the dipeptide BOC-Glu(αOBn)β-Ala. The last step was analogous to the coupling described above for compound **1**. A 1.03 g portion (2 mMol) of the dipeptide was reacted with an equimolar amount of APTES to yield 1.16 g (95%) of **2**.

IR: $\nu_{[NH}$ 3200−3400 cm^{-1}, $\nu_{[CO]}$ 1645 cm^{-1}, $\nu_{[CO]}$ 1700 cm^{-1}, $\nu_{[CO]}$ 1710 cm^{-1}. ^{1}H NMR: 7.3 (5H, m, a); 5.6 (2H, m, b); 4.1 (1H, m, c); 2.1 (2H, m, d); 2.25 (2H, m, e); 5.4 (3H, m, f + i + o); 2.4 (2H, m, g); 3.5 (2H, m, h), 3.2 (2H, m, j); 1.65 (2H, m, k); 0.65 (2H, m, l); 4.4 (6H, q, J = 6.8 Hz, m); 1.2 (9H, t, J = 6.8 Hz, n); 1.43 (9H, s, p).

*(c) BOC−Phe-APTES (**3**).* A 0.531 g portion (2 mMol) of

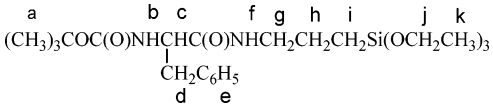

(BOC)Phe was coupled with 2 mMol of APTES under the same conditions as described under (*a*) for **1**. The reaction yielded 0.91 g (97%) of ***3*** under the form of a white paste.

IR: $\nu_{[NH]}$ 3200−3400 cm^{-1}, $\nu_{[CO]}$ 1645 cm^{-1}, $\nu_{[CO]}$ 1700 cm^{-1}. ^{1}H NMR ($CDCl_3$): 1.43 (9H, s, a); 5.7 (2H, m, b + f); 3.5 (1H, m, c); 5.4 (2H, m, d); 7.2 (5H, m, e); 3.2 (2H, m, g); 1.65 (2H, m, h); 0.65 (2H, m, i); 4.4 (6H, q, J = 6.8 Hz, j); 1.2 (9H, t, J = 6.8 Hz, k).

2.2. Mesoporous Preparation. The fluorinated surfactant used (provided by DuPont) had an average chemical structure of $CF_3(CF_2)_7C_2H_4(OC_2H_4)_9OH$, labeled as $R^F_8(EO)_9$ (or FSN-100, its commercial name). Indeed, its hydrophilic chain moiety exhibited a Gaussian chain length distribution. To synthesize the functionalized materials, first a micellar solution of $R^F_8(EO)_9$ at 10 wt % in water was prepared. Then the silica sources were added, with the surfactant/silica molar ratio being fixed to 0.5. The organosilane/(organosilane + TMOS) molar fraction (noted r) was varied from 0.02 to 0.10. The gel obtained was sealed in Teflon autoclaves and heated for 1 day at 80 °C. The final products were recovered after ethanol extraction with a Soxhlet apparatus for 30 h.

2.3. Mesoporous Characterization. X-ray measurements were carried out using a home-built apparatus equipped with a classical tube (λ = 1.54 Å). The X-ray beam was focused by means of a curved gold/silica mirror on the detector placed at 527 mm from the sample holder. Nitrogen adsorption−desorption isotherms were obtained at −196 °C over a wide relative pressure range from 0.01 to 0.995 with a volumetric adsorption analyzer TRISTAR 3000 manufactured by Micromeritics. The samples were degassed further under vacuum for several hours at room temperature before nitrogen adsorption measurements. The pore diameter and the pore size distribution were

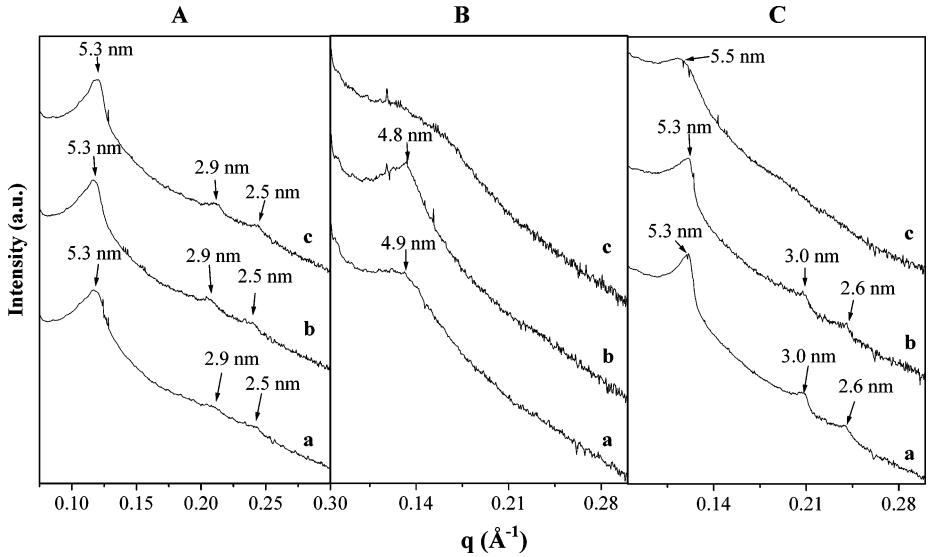

Figure 2. SAXS patterns of samples functionalized with BOC-Phe-APTES (A), Z-Asp(αOBn)-APTES (B), and BOC-Glu(αOBn)-βAla-APTES (C) (a, $r = 0.02$; b, $r = 0.05$; and c, $r = 0.10$).

determined by the BJH (Barret−Joyner−Halenda) method.[32] The IR spectra were recorded on a Perkin-Elmer (Spectrum one) FTIR spectrometer in transmission mode (KBr pellets). No treatment was performed to evacuate water.

3. Results and Discussion

3.1. Structural Investigation. Figure 2A, B, and C report the SAXS patterns of materials prepared, respectively, with BOC-Phe-APTES (Figure 2A), Z-Asp(αOBn)-APTES (Figure 2B), and BOC-Glu(αOBn)-βAla-APTES (Figure 2C) at different values of r. It has been reported[33] that X-ray diffractograms of powdery hexagonal mesoporous materials exhibit a typical three-peak pattern with a very strong feature at a low angle (100 reflection line) and two other weaker peaks at higher angles (110 and 200 reflection lines). For materials functionalized with BOC-Phe-APTES (Figure 2A) or with values of r inferior to 0.1 for BOC-Glu(αOBn)-βAla-APTES (Figure 2C lines a and b), in addition to a sharp peak at 5.3 nm, two other peaks located at 3.0 and 2.6 are detected on the SAXS pattern. As mentioned above, the presence of the last two peaks is characteristic of a hexagonal organization of the channels. The unit cell a_0, which is the sum of the pore diameter and the thickness of the pore wall, can be deduced from the relation $a_0 = 2d_{100}/(3)^{1/2}$ and its value is equal to 6.1 nm. The wall thickness (Table 2) is deduced by subtracting the pore size determined by the BJH method (see below) from the dimension of the unit cell.

The hexagonal arrangement of the channels is further confirmed by TEM micrographs of different samples (Figure 3a−c). The Fourier transform pictures of TEM images exhibit 6-fold symmetry and the measured angles between two bright spots are very close to 60° (Figure 3a and b insert). Two light spots (Figure 3c insert) are present, indicative of the parallelism of well-oriented channels.

Table 2. Mesoporous Materials: Structure, Values of *d* spacing, Cell Parameter (a_0), Specific Surface Area (S_{BET}), Pore Diameter (∅), Pore Volume (V_p), and Wall Thickness as a Function of the Organosilane/(Organosilane + TMOS) Molar Ratio (r)

r	structure	d-spacing (nm)	a_0 (nm)	S_{BET} (m^2/g)	∅ (nm)[a]	V_p (cm^3/g)[a]	wall thickness (nm)[b]
			BOC-Phe-APTES				
0.02	hexagonal	5.3	6.1	858	3.4	0.760	2.7
0.05	hexagonal	5.3	6.1	813	3.6	0.792	2.5
0.10	hexagonal	5.3	6.1	983	3.4	0.982	2.7
			Z-Asp(αOBn)-APTES				
0.02	wormhole	4.9		732	<1.7	0.365	
0.05	wormhole	4.8		690	<1.7	0.350	
0.10	wormhole			592	<1.7	0.222	
			BOC-Glu(αOBn)-βAla-APTES				
0.02	hexagonal	5.3	6.1	[c]	[c]	[c]	[c]
0.05	hexagonal	5.3	6.1	676	5.4	1.158	0.7
0.10	wormhole	5.5		609	5.1	1.040	0.4

[a] Values obtained from BJH method applied to the adsorption branch of the isotherm. [b] Values obtained by subtracting pore diameter from cell parameter. [c] Data not available.

For BOC-Glu(αOBn)-βAla-APTES, if the ratio r is further increased to more than 0.05, secondary reflections are no longer detected (Figure 2C, line c), meaning that the regular channel array is lost; the presence of a single reflection indicates the formation of a disordered structure. In this case, the mesoporous molecular sieve exhibits a wormhole-like channel system, analogous to that of MSU-type materials. The broad peak observed on the XRD pattern is an indication of the average pore-to-pore separation in the disordered wormhole framework, which presents a lack of long-range crystallographic order. The value of the pore wall thickness (Table 2) depends strongly on the nature of the organic group. For example, for a ratio r of 0.05 the pore wall thickness value varies from 2.5 (BOC-Phe-APTES) to 0.7 nm (BOC-Glu(αOBn)-βAla-APTES).

With Z-Asp(αOBn)-APTES as functional group, whatever the organosilane/(organosilane + TMOS) molar fraction, only wormhole-like structures are recovered. The wormhole structure is also confirmed by TEM (Figure 3d).

(32) Barret, E. P.; Joyner, L. G.; Halenda, P. P. *J. Am. Chem. Soc.* **1951**, *73*, 37.
(33) Chen, C. Y.; Xiao, S. O.; Davis, M. E. *Microporous Mater.* **1995**, *4*, 20.

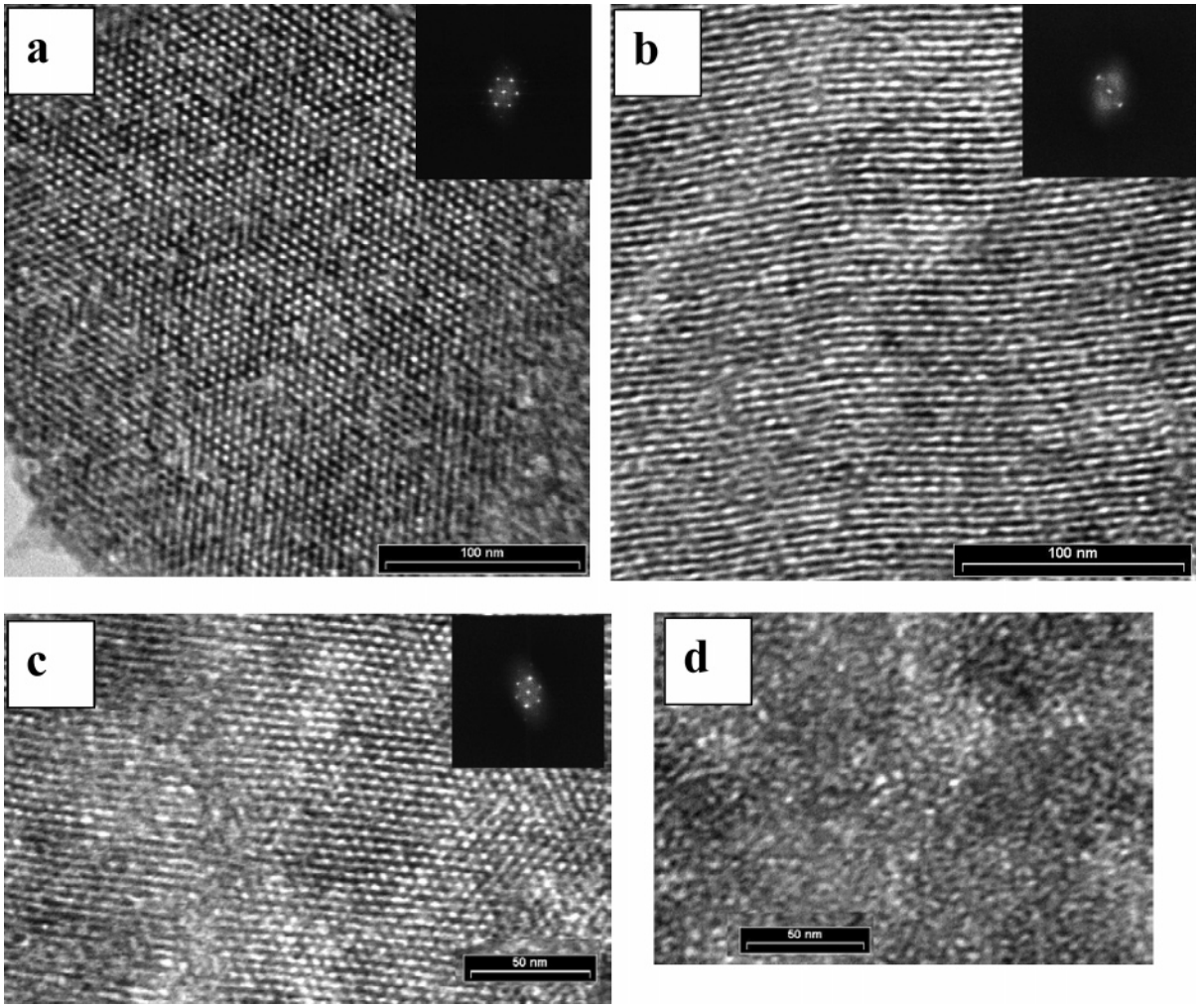

Figure 3. TEM micrographs and Fourier transform of samples functionalized with BOC-Glu(αOBn)-βAla-APTES (a, $r = 0.02$), BOC-Phe-APTES (b and c, $r = 0.10$), and Z-Asp(αOBn)-APTES (d, $r = 0.05$).

Results obtained by SAXS measurement clearly evidenced that the channel array depends strongly on the nature of the functional group and on the value of r. There is an optimum range of the organosilane/(organosilane + TMOS) molar ratio that can be employed to synthesize functionalized mesoporous materials with a well-ordered channel arrangement.

3.2. Characterization by Nitrogen Adsorption−Desorption. The nonfunctionalized mesoporous silica materials, prepared for comparison, exhibit a type IV isotherm (Figure 4), according to the BDDT classification.[34] The adsorption branch of the isotherm can be decomposed into three parts: the monolayer; multiple adsorption of N_2 on the wall of the mesopores, i.e., the capillary condensation of nitrogen within the mesopores; and then the saturation. An H_1 type hysteresis loop in which adsorption and desorption branches are steep[35] is observed for this sample. The specific surface area and pore volume values are, respectively, 883 m^2/g and 1.36 cm^3/g. The pore diameter distribution determined by using the BJH method is quite narrow and centered at ca. 4.6 nm (Figure 4, insert).

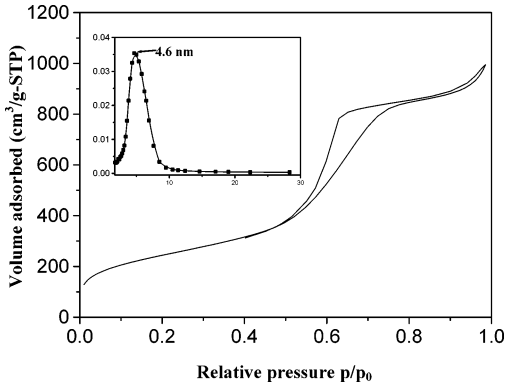

Figure 4. Nitrogen adsorption−desorption isotherm and pore size distribution (insert) of the nonfunctionalized mesoporous materials.

The nitrogen adsorption−desorption isotherms of the functionalized materials are shown in Figure 5. For all values of r, compounds functionalized with BOC-Phe-APTES (Figure 5A) and BOC-Glu(αOBn)-βAla-APTES (Figure 5C) display a type IV isotherm. The pore-size distribution analysis reveals that the pore diameter depends strongly on the nature of the organic group. Indeed, materials prepared with BOC-Phe-APTES exhibit a narrow pore size distribution, centered at 3.4 nm, whereas for molecular sieves synthesized with BOC-

(34) Brunauer, S.; Deming, L. S.; Deming, W. S.; Teller, E. *J. Am. Chem. Soc.* **1940**, *62*, 1723.
(35) Gregg., S. I.; Sing, K. S. W. *Adsorption, Surface Area and Porosity*, 2nd ed.; Academic Press: London, 1982.

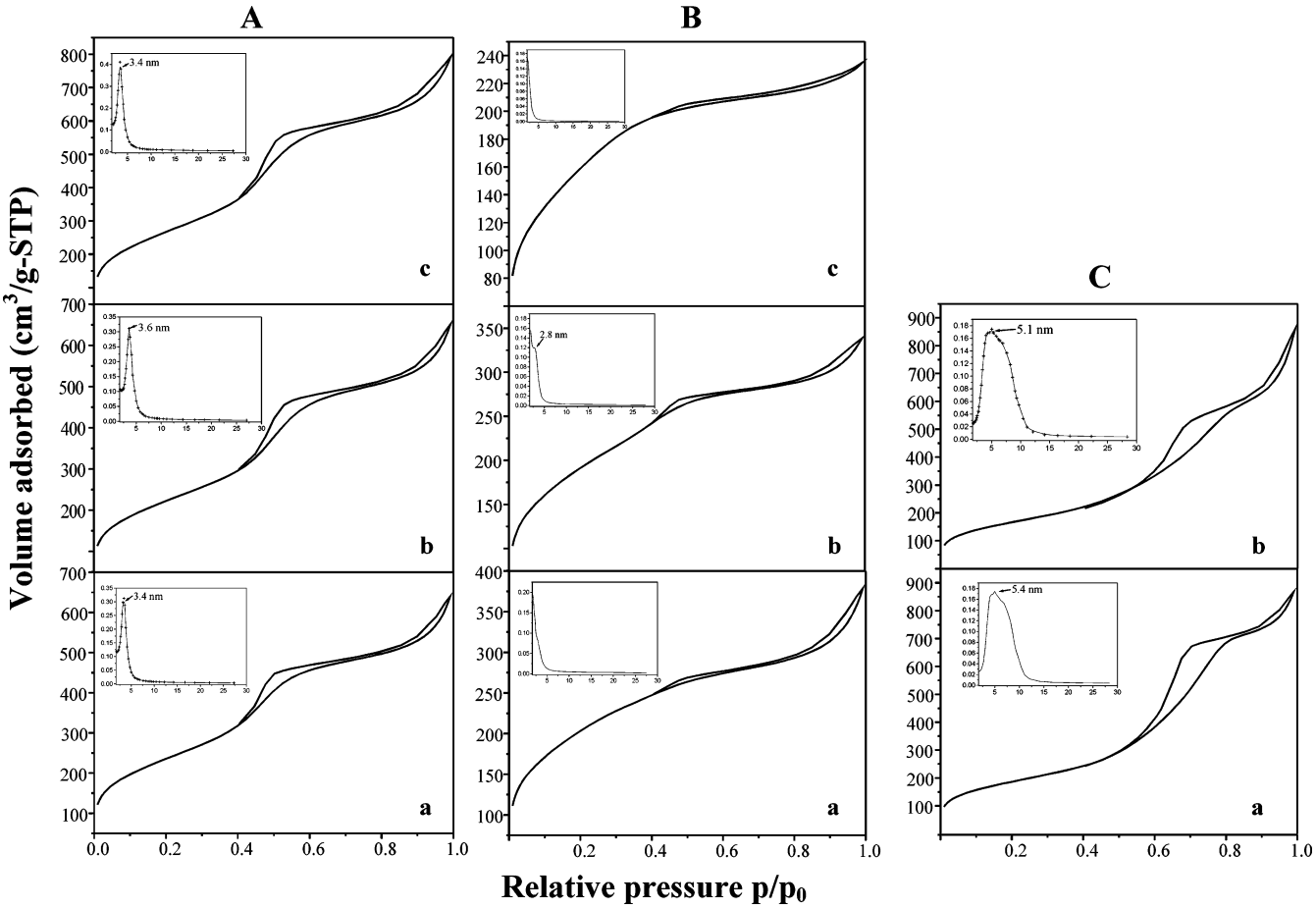

Figure 5. Nitrogen adsorption−desorption isotherms and pore size distribution (insert) of samples functionalized with BOC-Phe-APTES (A) and Z-Asp(αOBn)-APTES (B) (a, $r = 0.02$; b, $r = 0.05$; and c, $r = 0.10$), and BOC-Glu(αOBn)-βAla-APTES (C) (a, $r = 0.05$; b, $r = 0.10$.

Glu(αOBn)-βAla-APTES, the pore size distribution is broader and its maximum is shifted toward higher value (5.4 nm). In a general way, specific surface area and pore volume values of functionalized silica are lower than those of the pure mesoporous silica materials (Table 2). This phenomenon can be attributed to the occupancy of the mesopore channels by the organic groups.

For samples functionalized with Z-Asp(αOBn)-APTES, the situation is quite different. Nitrogen adsorption−desorption isotherms (Figure 5B) of all samples obtained are not well defined. This kind of isotherm is situated between type I, related to microporous materials, and type IV, characteristic of mesoporous materials. In agreement with Dubinin,[36] we can conclude that these materials possess supermicropores, i.e., pores with sizes ranging from 1.5 to 2.0 nm. Those compounds have low specific area and pore volume values, reflecting the poor degree of the channel array organization.

In any case, it should be noted that the adsorbed volume of nitrogen increases significantly at high relative pressures instead of remaining constant due to saturation. These compounds show very large secondary mesoporosity or even macroporosity. These latter could stem from the interparticle pores. The condensation of nitrogen in these large mesopores or macropores occurs very likely in addition to the adsorption inside the channels. Nevertheless, as this supplementary textural porosity is observed for the nonfunctionalized materials (Figure 4), its origin cannot be due to the functionalization process and should rather be related to the conditions of synthesis, and in particular to the pH value. Indeed, for the analogous hydrogenated system $C_{16}(EO)_{10}$ in a paper dealing with the effect of pH of the synthesis gel on the preparation of mesoporous silica, we have reported[37] that a considerable amount of secondary porosity appears upon pH increase. The appearance of secondary or interparticular porosity has been correlated with the SEM observations that show the formation of very small particles with increasing pH values of the synthesis gel. However, it cannot be completely excluded that a second amorphous material may be responsible for this effect.[38]

3.3. Efficiency of Functionalization. *3.3.1. IR Spectroscopy.* The framework of mesoporous silica materials consists of SiO_4 tetrahedra, which are joined by oxygen atoms. The FTIR spectra of the materials obtained, recorded in the 450−4000 cm^{-1} frequency domain are depicted in Figure 6. The observed bands

(36) Dubinin, M. M. In *Progress in Surface and Membrane Science*, Vol. 9; Cadenhead, D. A., Ed.; Academic Press: New York, 1975; p 1.

(37) Leonard, A.; Blin, J. L.; Jacobs, P. A.; Grange, P.; Su, B. L. *Microporous Mesoporous Mater.* **2003**, *63*, 59.

(38) Caldararu, H.; Caragheorgheopol, A.; Savonea, F.; Macquarrie, D. J.; Gilbert, B. C. *J. Phys. Chem. B* **2003**, *107*, 6032.

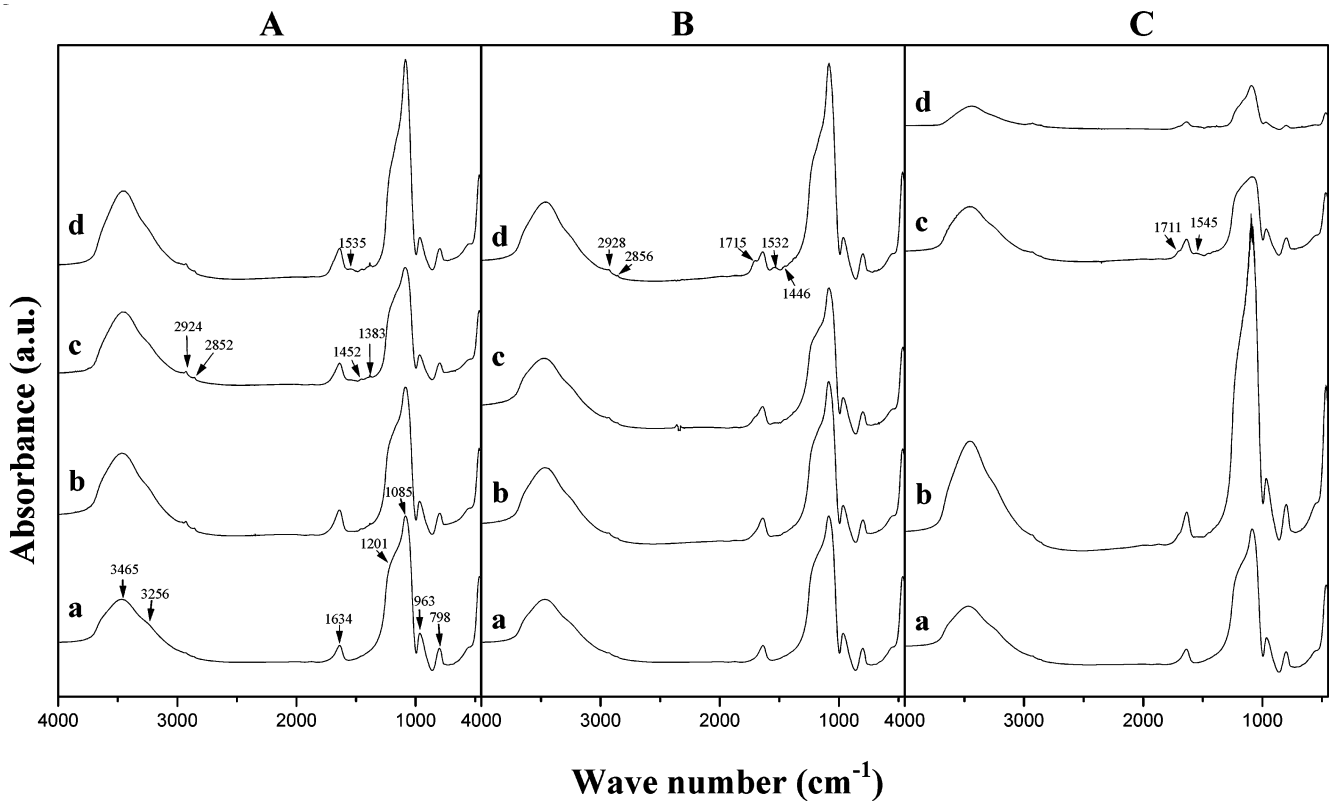

Figure 6. FTIR spectra of the pure mesoporous materials (a) and samples functionalized with BOC-Phe-APTES (A), Z-Asp-(αOBn)-APTES (B), and BOC-Glu(αOBn)-β-Ala-APTES (C) (b: $r = 0.02$; c: $r = 0.05$; and d: $r = 0.10$).

were assigned according to results published in the literature.[39]

The nonfunctionalized silica molecular sieve exhibits bands located at 3465, 3256, 1634, 1201, 1085, 963, and 798 cm^{-1} (Figure 6A, line a). The most intensive band, centered at 1085, and the shoulder at 1201 cm^{-1} are associated with the SiO_4 $\nu_3(F_2)$ stretching vibration. The band at 798 cm^{-1} corresponds to the SiO_4 $\nu_1(A)$ stretching vibration. The bands at 3465, 3256, and 1634 cm^{-1} are attributed to the stretching (3465 and 3256 cm^{-1}) and bending (1634 cm^{-1}) vibrations of water molecules adsorbed on the surface of the mesoporous materials. The band at 963 cm^{-1} is related to the Si−(OH) stretching of terminal silanol.

FTIR spectra of functionalized silica exhibit quite similar features. Indeed, in addition to the bands of the silica framework reported above, we observe vibrations that can be assigned as follows: bands detected at 2924 and 2852 cm^{-1} are attributed to the stretching vibrations of the CH group, whereas those at 1452 and 1383 cm^{-1} are due to the bending vibrations of this group. The band detected at around 1535 cm^{-1} (Figure 6A and B) or at 1545 cm^{-1} (Figure 6A, line c) can arise from either the stretching of the C=C bond of the aromatic rings or from the bending vibrations of NH groups. Moreover, for materials functionalized with Z-Asp-(αOBn)-APTES and BOC-Glu(αOBn)-β-Ala-APTES the functionalization is clearly evidenced by the band located at around 1715 cm^{-1}, which is unambiguously attributed to the C=O stretching vibration. Its intensity increases with the monomer loading. Results obtained by IR spectroscopy prove the efficiency of the functionalization of the mesoporous silica.

3.3.2. ^{29}Si and ^{13}C MAS NMR. Solid state ^{29}Si MAS NMR spectra provide information about the silicon environment and about the degree of functionalization with the organic groups. The ^{29}Si MAS NMR spectrum of the nonfunctionalized molecular sieves consists of signals at −91, −101, and −111 ppm (Figure 7a). These peaks are, respectively, due to Q^2 [$Si(OSi)_2(OH)_2$], Q^3 [$Si(OSi)_3OH$], and Q^4 [$Si(OSi)_4$] sites.[40] In addition to these three peaks, spectra of mesoporous functionalized materials display two more resonances at $\delta = -56$ and $\delta = -66$ ppm (Figure 7), assigned, respectively, to T^2 [$(SiO)_2Si(OH)Y$] and T^3 [$(SiO)_3SiY$].[41,42] These peaks are attributed to the Si atoms covalently bound to organic substituents; their intensity increases with the loading of functional groups. These observations confirm that the organic groups have been readily incorporated into the mesoporous structure. Spectra were deconvoluted (Figure 8) in order to determine the relative areas of the various peaks. Indeed, the relative integrated intensities of the siloxane (Q^n, $n = 2, 3, 4$) and organosilane (T^m, $m = 2, 3$) allow the quantitative assessment of the incorporation of organic moieties. The loading with functional groups can be estimated to be equal to $T^m/(T^m + Q^n)$. Results, summarized in Table 3, indicate that the amount of organic groups incorporated in materials corresponds, within the limits of

(39) Kirov, N.; Simova, P. *Vibrational Spectroscopy of Liquid Crystals*; Publishing House of the Bulgarian Academy of Sciences: Sofia, 1984.

(40) Kolodziejski, W.; Corma, A.; Navarro, M. T.; Perez-Pariente, J. *Solid State Nucl. Magn. Reson.* **1993**, *2*, 253.

(41) Sindorf, D. W.; Maciel, G. E. *J. Am. Chem. Soc.* **1983**, *105*, 3767.

(42) Lindner, E.; Schneller, T.; Auer, F.; Mayer, H. A. *Angew. Chem., Int. Ed.* **1999**, *38*, 2155.

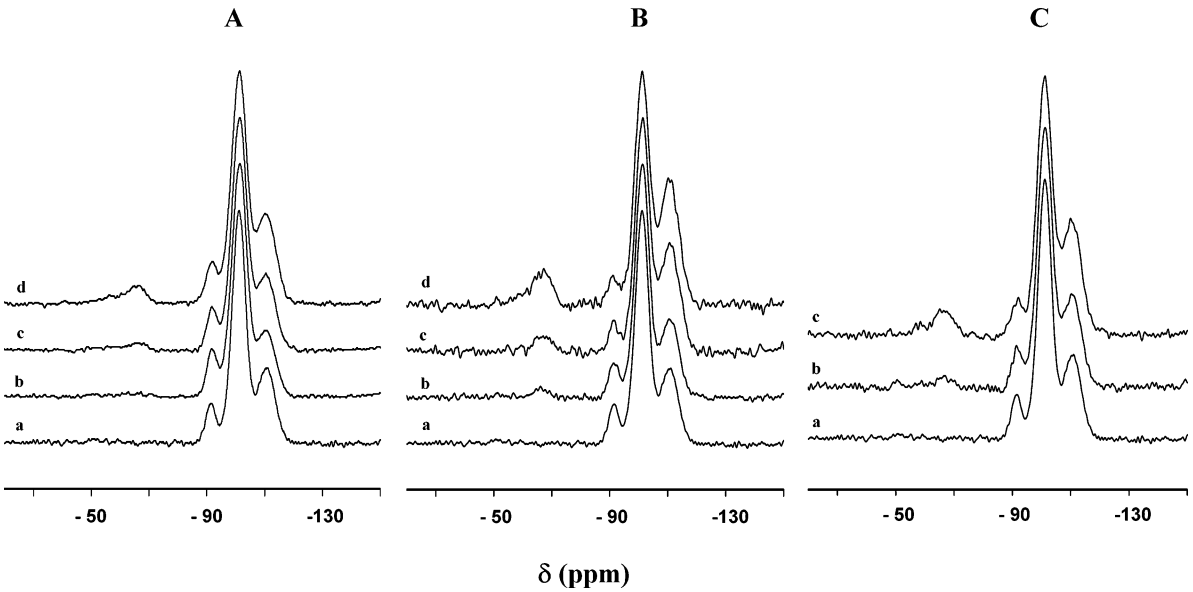

Figure 7. ^{29}Si NMR spectra of the pure mesoporous materials (a) and samples functionalized with BOC-Phe-APTES (A) and Z-Asp(αOBn)-APTES (B) (b, $r = 0.02$; c, $r = 0.05$; and d, $r = 0.10$), and BOC-Glu(αOBn)-βAla-APTES (C) (b, $r = 0.05$; c, $r = 0.10$).

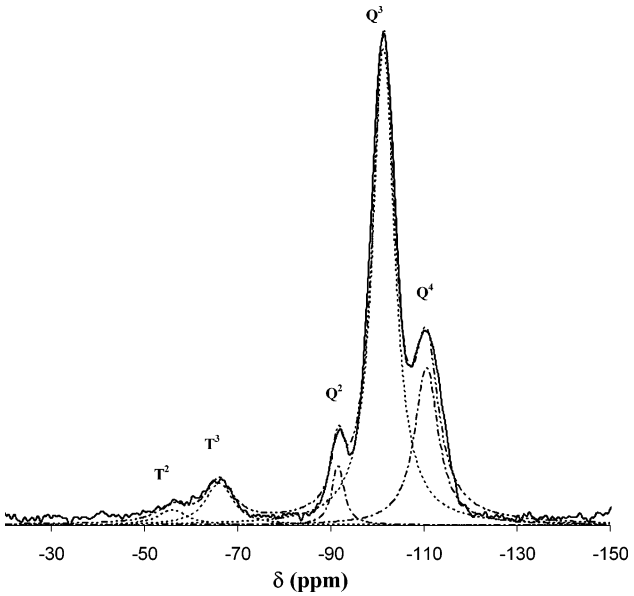

Figure 8. Deconvoluted ^{29}Si MAS NMR spectra of a representative functionalized silica.

experimental uncertainty, to the stoichiometry of the synthesis gel.

Figure 9 shows the ^{13}C MAS NMR spectra of the functionalized mesoporous molecular sieves. The attribution of the resonance peaks is summarized in Table 4. They are due to different carbon environments in the organosilane and reflect the incorporation of functional groups.

3.4. Discussion. Mesoporous materials have been prepared with a concentration of $R^F_8(EO)_9$ at 10 wt % in water. According to the phase diagram established for $CF_3(CF_2)_7C_2H_4(OC_2H_4)_9OH$,[31] this concentration corresponds to a micellar phase (L_1). The fact that the value of the organosilane/(organosilane + TMOS) molar fraction determined by ^{29}Si MAS NMR is in good agreement with the value in the synthesis gel shows that polymerization rates of organosilane and TMOS must be very close to each other. Therefore, the formation of the well-defined hexagonal array of the functionalized materials

Table 3. Relative intensities (%) of T^m(m = 2, 3) and Q^n(n = 2, 3, 4) signals

r in the synthesis gel	T^2 (%)	T^3 (%)	Q^2 (%)	Q^3 (%)	Q^4 (%)	$T^m/(T^m + Q^n)$
BOC-Phe-APTES						
0.02	-[a]	-	-	-	-	-
0.05	1.3	4.4	5.7	3.0	66.1	0.06
0.10	3.4	8.1	2.6	56.8	29.0	0.11
Z-Asp(αOBn)-APTES						
0.02	0.7	1.5	4.4	74.1	19.3	0.02
0.05	2.1	3.6	3.8	68.6	22.0	0.06
0.10	2.8	7.1	4.3	63.1	22.7	0.10
BOC-Glu(αOBn)-βAla-APTES						
0.02	0.0	2.2	2.4	70.1	25.2	0.02
0.05	0.0	5.2	1.7	58.1	34.9	0.05
0.10	0.3	10.7	1.6	53.3	34.1	0.11

[a] -: data not available.

prepared with BOC-Phe-APTES and BOC-Glu(αOBn)-βAla-APTES can be explained by the CTM-type mechanism (cooperative templating mechanism).[43−45] When the silylated monomers and TMOS are added to the micellar surfactant solution, hydrogen-bonds between the oxygen atoms of the oxyethylene groups of the surfactant and the hydrogen atoms of TMOS or organosilane are formed. To complete the polymerization of tetramethoxysilane and organosilane, these rodlike supramolecular assemblies (template−silica) rearrange themselves in regular stacks, leading to the formation of a hexagonal hybrid mesophase. After surfactant removal, mesoporous molecular sieves with a hexagonal channel array are obtained (Figure 10A). The pore diameter and the wall thickness, however, depend on the functional group. Under these conditions, the behavior of the surfactant in aqueous solution is the driving force in the formation of the regular array. If the loading of

(43) Zhao, D.; Huo, Q.; Feng, J.; Chmelka, B. F.; Stucky, G. D. *J. Am. Chem. Soc.* **1998**, *120*, 6024.
(44) Firouzi, A.; Kumar, D.; Bull, L. M.; Besier, T.; Sieger, P.; Huo, Q.; Walker, S. A.; Zasadzinski, J. A.; Glinka, C.; Stucky, G. D. *Science* **1995**, *267*, 1138.
(45) Lee, Y. S.; Sujardi, D.; Rathman, J. F. *Langmuir* **1996**, *12*, 6202.

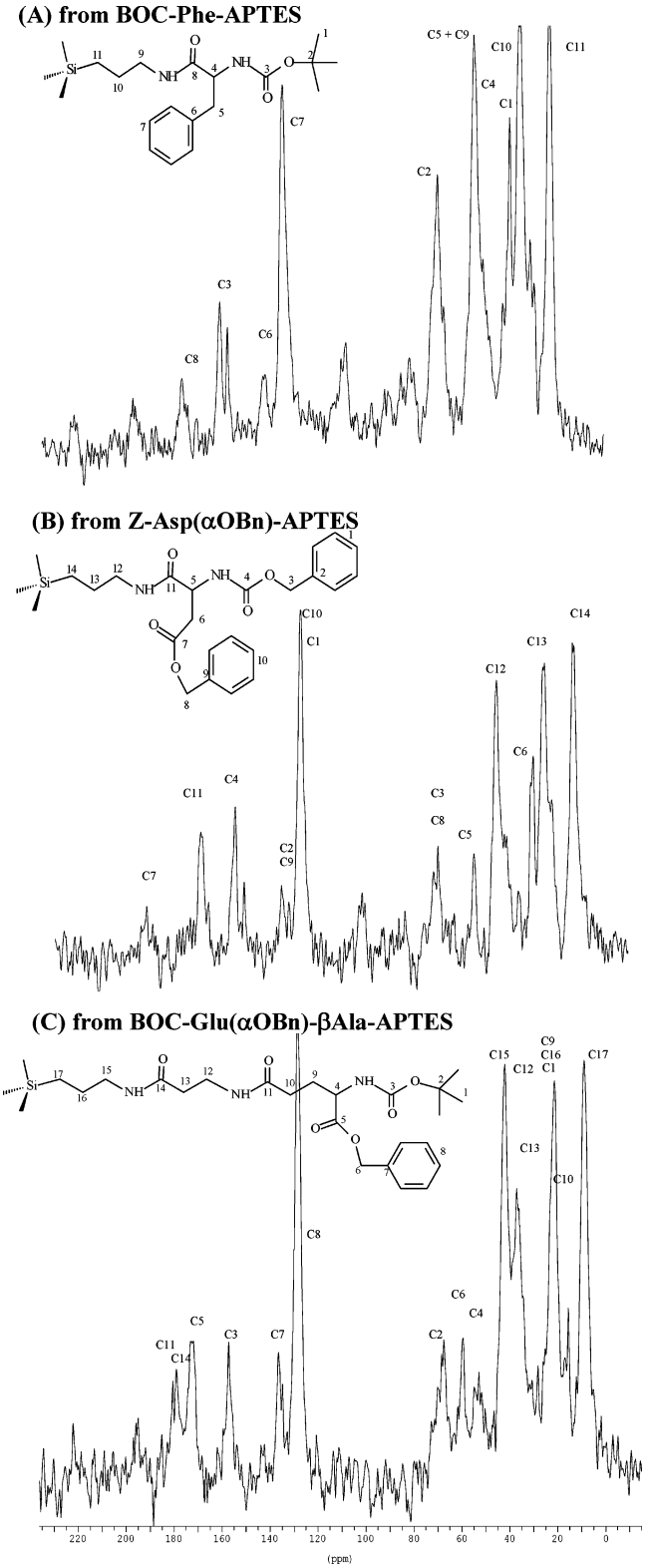

Figure 9. ^{13}C NMR spectra of samples functionalized with BOC-Phe-APTES (A), Z-Asp(αOBn)-APTES (B), and BOC-Glu(αOBn)-βAla-APTES (C) ($r = 0.10$).

BOC-Glu(αOBn)-βAla-APTES is increased, a wormhole-like structure is obtained (Figure 10B). In a paper dealing with the direct synthesis of functionalized mesoporous silica in the presence of a nonionic alkylpoly(ethylene oxide) surfactant using tetraethoxysilane and organotrialkoxysilane as silica sources, Richer et al.[23] explained that lypophilic interactions between the organosilane molecules and the hydrophobic core of the micelles are likely to result in a deeper penetration of the organosilane molecules into the micelles as compared to TEOS. The perturbations caused in the micelle organization lead therefore to more disordered materials. As the steric occupancy of BOC-Glu(αOBn)-βAla-APTES is higher than that of BOC-Phe-APTES, we can consider that such a phenomenon occurs also with increasing BOC-Glu(αOBn)-βAla-APTES loading.

Table 4. ^{13}C Chemical Shifts of Organic Groups Obtained from Solid State MAS NMR Spectra

BOC-Phe-APTES		Z -Asp(αOBn)-APTES		BOC-Glu(αOBn)-βAla-APTES	
	δ_C[a]		δ_C[a]		δ_C[a]
C1	26.8	C1	128.7	C1	21.4
C2	75	C2	133.7	C2	67.4
C3	156.7	C3	68.3	C3	157.2
C4	59.2	C4	157.3	C4	50.5
C5	42.8	C5	52.5	C5	171.9
C6	137.5	C6	37.5	C6	59.4
C7	128.8	C7	172.5	C7	136.5
C8	173.6	C8	68.3	C8	128.6
C9	42.5	C9	132.5	C9	29.5
C10	21.9	C10	128.5	C10	37.1
C11	9.1	C11	172.3	C11	179
		C12	42.5	C12	42
		C13	21.5	C13	37
		C14	9.3	C14	180
				C15	52
				C16	42.1
				C17	9

[a] δ_C in ppm from TMS.

Concerning materials functionalized with Z-Asp(αOBn)-APTES, the situation is quite different. Whatever the organosilane/(organosilane + TMOS) molar fraction, only disordered silicas with low specific surface areas are obtained. No pore size distributions in the mesoporous range are obtained by nitrogen adsorption−desorption analysis. As mentioned above, the functional loading in the synthesis gel is very similar to that calculated from the ^{29}Si MAS NMR data; therefore, the difference in behavior cannot be related to a difference in the polymerization rate between the organosilane and TMOS. Due to the presence of the two phenyl groups we may consider that Z-Asp(αOBn)-APTES is more hydrophobic than BOC-Phe-APTES and BOC-Glu(αOBn)-βAla-APTES; therefore, when the former monomer is added to the micellar solution, the overall hydrophobicity of the system increases. As a consequence, micelles can no longer be formed and only isolated molecules or aggregates of surfactant will be present in the solution. The CTM-type mechanism is no longer valid and materials with a randomly oriented pore structure and low surface area are recovered (Figure 10C).

4. Conclusions

The functionalization of mesoporous silica materials by the co-condensation method was investigated. Materials functionalized with BOC-Phe-APTES or with small amounts of BOC-Glu(αOBn)-βAla-APTES (molar fraction of organosilane/(organosilane + TMOS) inferior to 0.1) exhibit a hexagonal channel array. Higher BOC-Glu(αOBn)-βAla-APTES loading leads to a wormhole-like mesostructure. Whatever the organosilane/(orga-

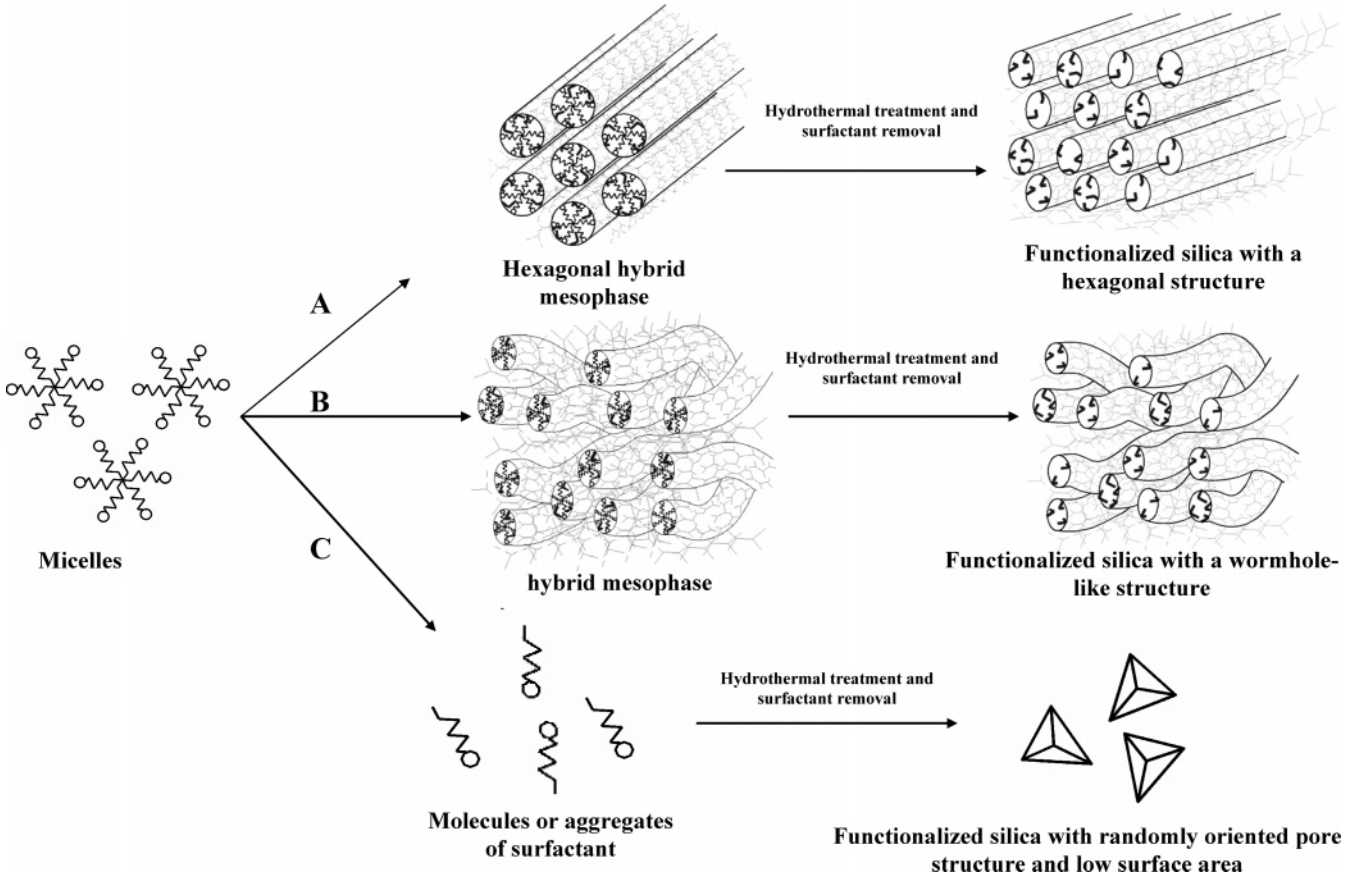

Figure 10. Scheme of the proposed mechanism for the formation of functionalized mesoporous materials.

nosilane + TMOS) molar fraction, only disordered structures are recovered when functionalization is performed with Z-Asp(αOBn)-APTES and no pore size distribution in the mesopore range is detected. This difference in behavior is related to the variation in the overall hydrophobicity of the system.

Results obtained from FTIR spectroscopy and from ^{29}Si and ^{13}C MAS NMR indicate that the functional group is readily incorporated into the mesostructure. We have also evidenced that the pore wall thickness is strongly affected by the nature of the functional group, for example—keeping r equal to 0.05—its value varies from 0.7 nm (BOC-Glu(αOBn)-βAla-APTES) to 2.5 nm (BOC-Phe-APTES). The correlation between the structure of monomer and that of the mesoporous materials is the subject of more detailed studies.

Acknowledgment. We thank A. Collard and S. Dupont for their contribution to the synthesis and characterization of the mesoporous materials, as well as DuPont de Nemours Belgium for providing the R^F_8-$(EO)_9$ (FSN-100), and Dr. P. Tekely and C. Gardiennet for assistance during the solid state NMR experiments.

CM049452R